Applied Computer Science 2026, vol. 22, no. 1, pp. 184–198
https://doi.org/10.35784/acs_8247

Submitted: 2025-08-13 | Revised: 2025-09-24 | Accepted: 2025-12-12

Keywords: machine learning, random forest, optimisation, welding, mechanical properties, steel, microstructure

Szymon KARSKI [1], *Michał AWTONIUK* [2], *Mirosław SZALA* [1*]
[1] Lublin University of Technology, Poland, s95779@pollub.edu.pl, m.szala@pollub.pl
[2] Warsaw University of Life Sciences, Poland, michal_awtoniuk@sggw.edu.pl
[*] Corresponding author: m.szala@pollub.pl

Application of artificial intelligence methods to determine the optimal process parameters in resistance projection welding of steel nuts

Abstract

The study employed applied computer modelling to identify the optimal process parameters for resistance projection welding using the original procedure. The influence of technological parameters (welding power, welding time, electrode pressure) on the quality of 184 welded joints produced by resistance projection welding of steel nuts and S235JR steel plates was examined using computer modelling methods, specifically a combination of machine learning and an evolutionary algorithm. A tree-based model was used to identify relationships between signals, and a genetic algorithm for multi-criteria optimisation. The prepared joints were then examined to determine the impact of the welding parameters on the microstructure, Vickers hardness, and strength of the welded joints (as assessed by pull-off testing). The superior strength of the projection welding joints was achieved through short welding times and high power. Additionally, limited welding time effectively restricted the heat-affected zone, reducing weld hardness and improving the joint's plasticity. The original modelling process enables energy consumption (welding current) to be minimised while maximising joint strength, which was the main aim of the work. Finally, the set of optimised welding parameters selected by AI was verified through sample welding and strength testing, and this was confirmed through final strength testing experiments.

1. INTRODUCTION

Nowadays, computer modelling is applied in many industries, including various welding applications (Kik et al., 2020), welding related processes such as thermal spraying (Łatka et al., 2020), additive manufacturing of metallic structures (Korzeniowski et al., 2023), adhesive bonding (Kubit et al., 2023), fatigue life optimisation of the riveted joints (Masoudi Nejad et al., 2024), erosion resistance optimisation (Singh et al., 2024) or applications related to weldment testing (Sawa et al., 2021). The various resistance and pressure welding processes have been systematically studied in scientific literature. For example, Dziurka et al. (2025) studied resistance spot welding electrode wear, Han et al. (2021) optimised the shape of a square nut for better projection welding performance using FEM, and Hu et al. (2022) predicted resistance spot welding (RSW) quality using artificial intelligence modelling.

The combination of modelling and optimisation methods also yields promising results. Recent literature presents both generative approaches for optimisation of production metrics and classical evolutionary searches for combinatorial problems (Nasso Toumba et al., 2025; Sikora & Gryglewicz–Kacerka, 2023). This combination significantly facilitates the search for a set of technological parameters for the modelled process that allows the production of a product with specific properties. For example, in (Winiczenko et al., 2013) two evolutionary optimisation methods were combined with an SVM model to determine the parameters of friction welding to obtain a sample with the highest tensile strength. This was an example of single-criteria optimisation. Another example is the work Szala et al. (2020), where a neural model of the thermal spray process was used in combination with a genetic algorithm. The authors applied a multi-criteria optimisation process, taking into account various properties of the obtained sample, including hardness, porosity and cavitation wear resistance. Another example of the use of multi-criteria optimisation, this time in the form of

a non-dominated sorting genetic algorithm III, was proposed by Johnson et al. (2023). The process was resistance spot welding (RSW), and product quality was evaluated using four criteria: nugget diameter, tensile shear strength, peel strength, and mean dynamic contact resistance. Unlike the previously cited work, no machine learning model was used; instead, an interpolation method called kriging was applied. In industrial practice, ML directly reduces operating times – e.g., modelling the optimal measurement time for a probe on a machine tool (Jozwik et al., 2024).

Another interesting machine learning technique is model explanation. Various methods are available to evaluate the impact of an input variable on the model's output signal, both globally and locally. The paper by Russell et al. (2024) presents a comprehensive resistance spot welding (RSW) process model with 19 input signals, and then uses the Shapley additive explanation (SHAP) method to identify those with the greatest impact on weld quality metrics.

Resistance welding technologies have become increasingly prevalent in the automotive industry (Chuenmee et al., 2025; Stavropoulos & Sabatakakis, 2024). Modern car bodies contain over 300 components assembled by resistance welding, including nuts and bolts, highlighting the importance of this technology in modern production lines (Larsson, 2008). Projection welding, one of the methods frequently used for joining car bodies, has been systematically studied and modelled to produce high-quality nut-sheet welded joints (Koal et al., 2025; Mikno, 2018; Mikno et al., 2019).

Although resistance welding is well established, it is a process with a narrow range of optimal parameters that is highly dependent on technological variables and material properties (Mikno, 2018; Szala & Łukasik, 2018). Consequently, there is a growing interest in using artificial intelligence to optimise welding processes, particularly for predicting the parameters required to produce high-quality, reliable joints (Hu et al., 2022). Using artificial intelligence to predict welding parameters can spare R&D departments the need to conduct numerous physical weld-joint tests. However, due to the complexity of the process, many AI algorithms may struggle to accurately predict parameters such as the mechanical strength of the weld. For this reason, the current study uses neural networks, which can model complex and intricate data. The deep learning layers used in AI enable the discovery of data structures and hidden patterns linking variables, which is useful when relationships are not immediately apparent. However, neural networks are not a flawless solution: they perform poorly with small datasets and are prone to overfitting. Therefore, careful selection of the network architecture and preparation of the training dataset are essential when applying this method (Antosz et al., 2024).

Previously, the experimental or finite element method (FEM) was used to predict welding parameters, but it was slow, imprecise and time-consuming (Han et al., 2021; Nielsen et al., 2014). These methods relied on repeatedly generating samples to find optimal parameters, with the range determined by the experimenter's experience. Applying an artificial intelligence algorithm that can accurately predict output parameters from input parameters will accelerate the optimisation process and enhance joint quality. It will also assist in monitoring parameters when changes are needed (Drégelyi-Kiss, 2023). Preparing samples for strength testing is expensive and time-consuming. Preparing samples for strength testing is expensive and time-consuming, but artificial intelligence can accurately predict the results. However, it is difficult to find studies in which optimisation results were applied to welding and verified through experimentation. Therefore, this study aims to address this issue.

This study aimed to use methods from applied computer science to develop an algorithm that could optimise a set of parameters (welding power P, welding time t and electrode pressure p) for resistance projection welding of steel nuts and S235JR steel plates. The algorithm was trained and validated using experimental data to minimise energy consumption (welding current) while maximising joint strength. A combination of machine learning methods and evolutionary algorithms was employed to determine the optimal process parameters for projection welding. Finally, the set of optimised welding parameters selected by AI was verified through sample welding and strength testing. This study employed computer modelling to determine optimal resistance projection welding parameters and enhance their optimisation using the original procedure – the novel aspect of this research.

2. MATERIALS AND METHODS

The research steps were carried out in accordance with the diagram shown in Figure 1. A series of tests were conducted during the experiment to determine the influence of process parameters on joint quality. This

information was then used to develop a model that could predict weld output parameters based on input parameters.

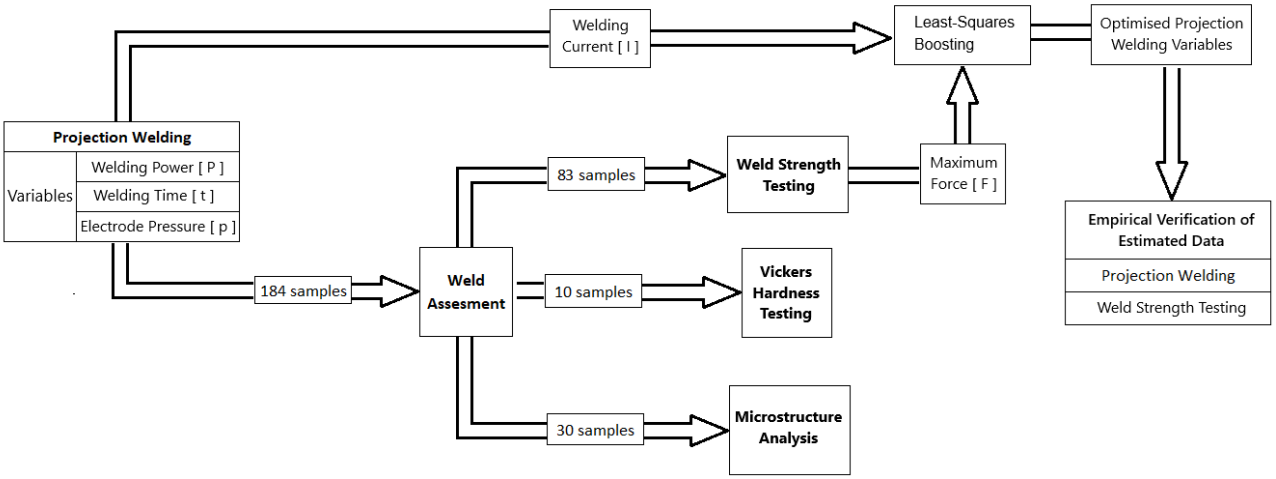

Fig. 1. Stages of the research conducted in this study

2.1. Tested materials and their preparation for welding

The experiment involved two main components: steel nuts and a steel sheet. These components were joined using resistance welding and tested. The materials were prepared to ensure the joint had the desired mechanical properties and to improve weld consistency. The joint samples were made from a 1 mm-thick S235JR grade steel sheet. For the experiment, rectangular pieces measuring 50 × 30 × 1 mm were cut from the sheet. Depending on whether the sheet was intended for welding an M4 or M5 nut, each sample had a 5 mm or 6 mm hole drilled in it. To remove imperfections from the drilling process, the sheets were sanded with abrasive paper. Just before welding, each sample was cleaned with extraction gasoline. M4 and M5 nuts, produced in accordance with the DIN 928 standard (see Figure 2), were employed in the welding process. The nuts were made of carbon steel.

Fig. 2. (a) Commercial nuts manufactured in accordance with DIN 928; (b and c) visualisation of M5 nuts used in the study

2.2. Projection welding process

Projection welding is a type of resistance welding in which current is concentrated at contact points created by small geometric projections on one or both parts. These projections concentrate heat and collapse to form weld nuggets (Wang & Zhang, 2017). Figure 3 illustrates the detailed process of projection welding.

Welding was performed using a PFB 126X PX1700 PRO resistance welding machine equipped with flat electrodes designed specifically for nut welding (Figure 4). The three main technological parameters that varied between each weld were welding time (t) (range: 20–1000 ms), electrode pressure (p) (range: 3.5–7.0 bar) and welding power (P) (expressed as a percentage of the machine's maximum power of 25 kW). A total of 184 welds were performed. After each weld, the welding current I generated by the machine was noted and used in the optimisation procedure described in Section 2.5.

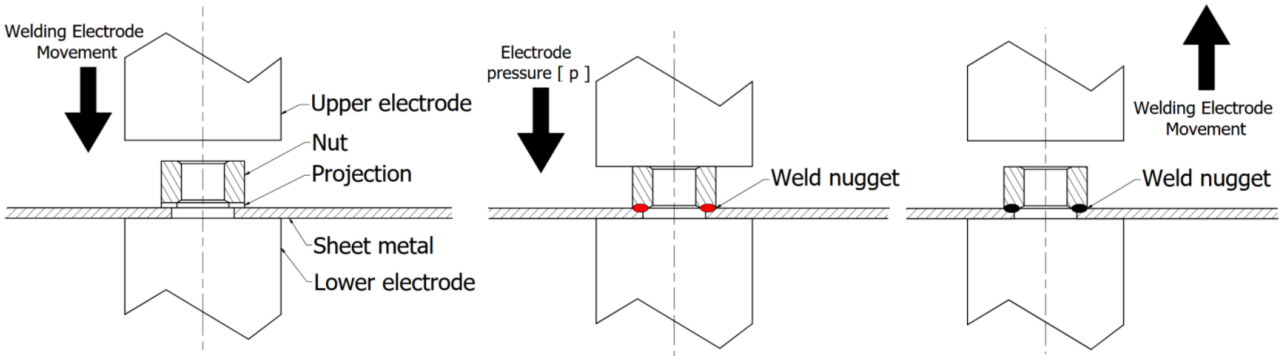

Fig. 3. The concept of projection welding: (a) the nut and sheet metal are positioned on the lower electrode and in preparation for welding; (b) the welding process involves the upper electrode pressing against the nut, allowing current to flow for a specified time; weld nuggets form at the nut projections; (c) the upper electrode is lifted away from the nut, completing the joint

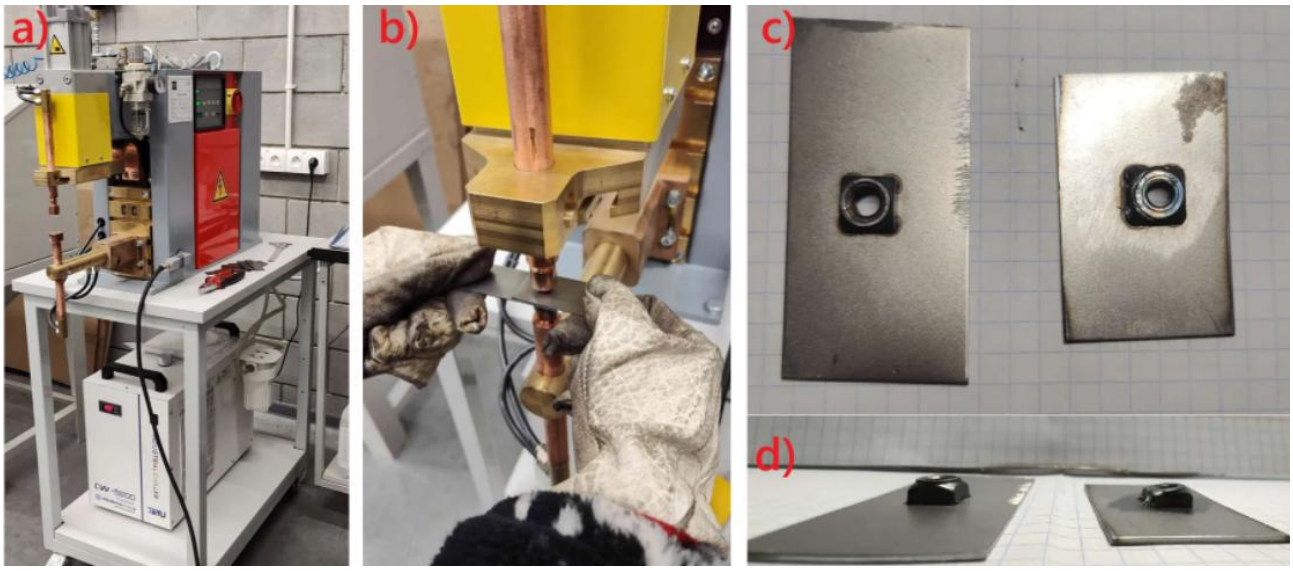

Fig. 3. (a) Welding machine; (b) welding process; (c and d) exemplary nut-sheet metal welded joints

2.3. The weld strength (pull-off testing)

To evaluate the quality of the weld under the selected welding process parameters, tests were performed to determine the strength of the welded joint. These tests were conducted using a Shimadzu AG-X Plus universal testing machine, according to the setup depicted in Figures 5 and 6. The punch pressed against the screw, transferring the load through the thread to the nut and generating a force that attempted to detach the nut from the welded sheet. To minimise the bending effect of the sheet providing support, a spacer sleeve was employed.

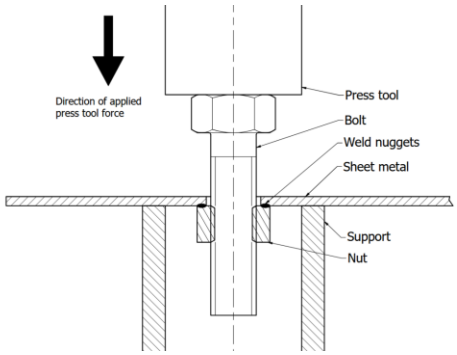

Fig. 4. Presentation of welded joint pull-off testing. Figure 4c and d show the exemplary test joints, while Figure 6 shows the equipment used for testing

The experiment involved the destructive testing of 83 welds. During the test, the force at which the nut detached from the sheet of metal was recorded. In most cases, the nut did not separate from the sheet and instead significant deformation of the sheet metal was observed. In these instances, the maximum force applied before the sheet exceeded its yield strength was recorded.

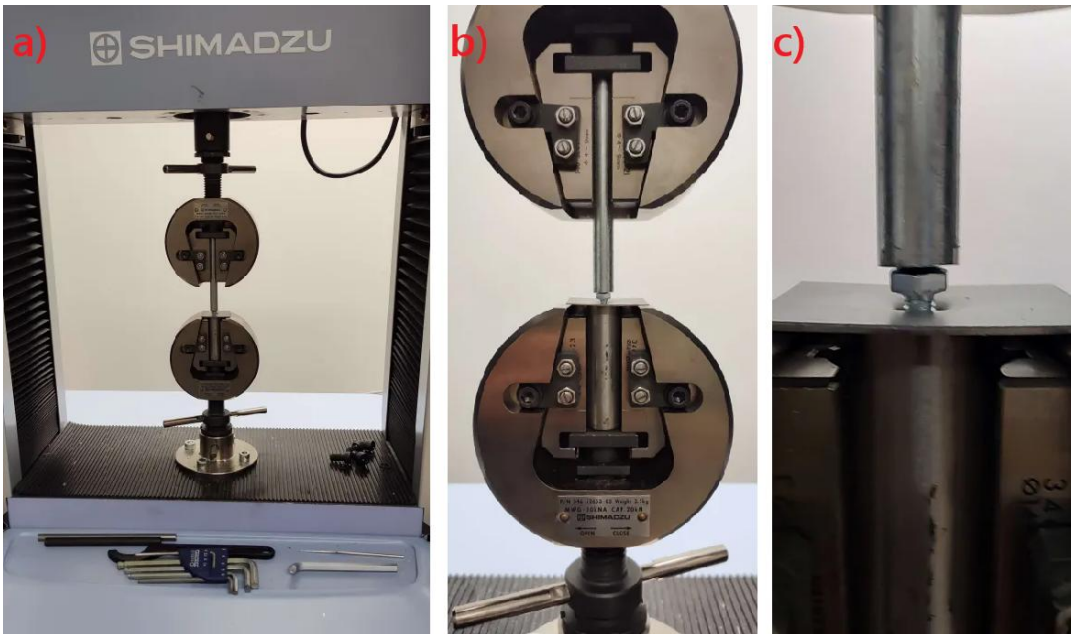

Fig. 5. (a) Pull-off test equipment; (b, c) exemplary testing of a nut-sheet joint according to the scheme given in Fig. 5

2.4. Macrostructural and hardness analysis

In order to determine the exact effect of the process parameters on the properties of the weld, a visual inspection, a metallographic analysis and a hardness test were conducted. The metallographic samples were prepared by cutting, grinding, polishing and etching the joint cross-sections, as illustrated in Figure 7. These samples were then subjected to macro- and microscopic metallographic analysis to evaluate weld quality (i.e. joint formation, dimensions and nut deformation rate), assess the heat-affected zone, and identify changes in the microstructure in specific weld nugget zones. The metallographic analysis was then performed using a scanning electron microscope (SEM) (Phenom Pro-X). Vickers hardness was investigated in the nut, the heat-affected zone (HAZ), the weld, and the sheet metal. Measurements were performed using the HV0.3 scale. To improve the accuracy, five measurements were taken on the weld, the nut and the sheet for each sample.

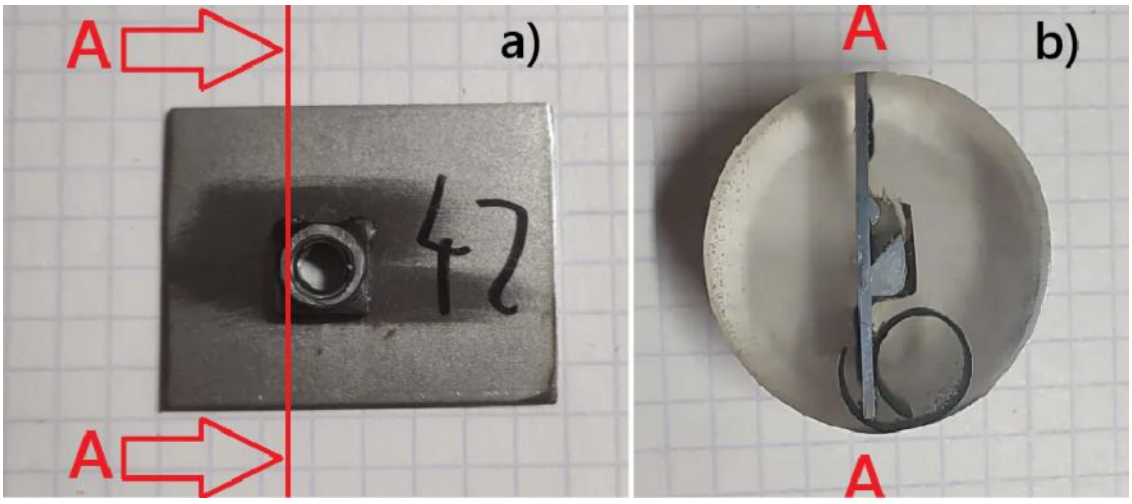

Fig. 6. (a) Projection-welded nut-sheet metal joint;
(b) preparation of a metallographic cross-section for microstructure and hardness analysis

2.5. Modelling and optimisation procedures

We used a boosted regression tree ensemble for modelling. These models were developed using the Least-Squares Boosting (LSBoost) algorithm (Breiman, 2001; Hastie et al., 2009), which will be used as the model name throughout the rest of this paper. LSBoost was developed using the Statistics and Machine Learning Toolbox in the MATLAB environment (version 2024a, MathWorks, Natick, MA, USA). We built two models with one output. The M_F model's output signal was the maximum force F (N), and the M_I model's output signal was the welding current I (kA). LSBoost models operating in multi-response regression mode have only been available in the MATLAB environment since version R2024b. Both models had the same four input signals: nut size; electrode pressure p (bar); welding power P (kW); and welding time t (ms). A block diagram of the model is shown in Figure 8.

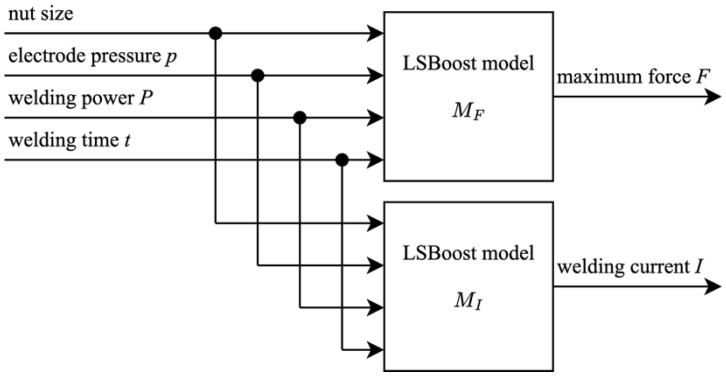

Fig. 7. Block diagram of the analysed LSBoost model

We selected training and test subsets in an 80:20 ratio from a dataset comprising 83 samples (41 M4 nuts and 42 M5 nuts). The original data balance was maintained in both subsets. During the learning process, we employed 10-fold cross-validation and optimised the model's hyperparameters via Bayesian optimisation. The objective of this optimisation was to minimise the mean squared error. We then evaluated the quality of the model using the mean absolute error (MAE) indicator.

Next, we used LSBoost models to determine the optimal parameters for the welding technology. This process was optimised using a multi-objective genetic algorithm (MOGA), which was implemented in the Global Optimisation Toolbox within the MATLAB environment. The vector of decision variables x is described by equation (1), and the optimal solution (2) should satisfy the inequality constraints (3).

$$x = [p, P, t]^T \tag{1}$$

$$x^* = [p^*, P^*, t^*]^T \tag{2}$$

$$\begin{cases} 3 \le p^* \le 8 \\ 12.5 \le P^* \le 25 \\ 20 \le t^* \le 1000 \end{cases} \tag{3}$$

The adopted ranges are based on technological considerations. The capabilities of the welding machine limited the maximum welding power (P) and the minimum welding time (t). The maximum pressure was limited by the electrode pressure control equipment: below 3 bar, the equipment lacked the power to lift the electrodes high enough to place a sample between them. With less than 12.5 kW of welding power, establishing a firm connection between the sheet metal and the nut was difficult, even with prolonged welding time. Where such a connection was achieved, the force required to break it was so small that the samples often broke during the cooling of the sheet metal. For welding times above 200 ms, the results were not repeatable; however, with sufficiently low power, it was possible to produce samples suitable for strength tests. At around 1000 ms, the samples began to deform significantly, even at very low power levels, which made it difficult or impossible to perform the strength test. We also incorporated the decision variable resolutions into the algorithm: 0.2 bar for electrode pressure (p), 0.125 kW for welding power (P) and 20 ms for welding time (t).

This is an example of multi-criteria optimisation, where the aim is to determine the optimal process parameters to produce a sample with maximum force (F) and minimum current (I). The optimisation task can be formulated as a complex objective vector function (J).

$$J(x) = [\max F(x), \min I(x)]^T \tag{4}$$

This optimisation aims to obtain a sample with a strength greater than the minimum yield strength of the sheet metal used in this test (approximately 235 MPa), while using the lowest possible current. This is because current is directly related to power usage, meaning that a sample using less current will also be cheaper to produce. The result of the MOGA algorithm is the Pareto front, i.e. a set of optimal solutions that satisfy the constraints given in equation (3) while optimising each element of the objective vector function J (4). The main MOGA parameters were as follows: number of generations = 30; population size = 100; selection type = tournament; crossover probability = 0.8. For a detailed description of the MOGA parameters, please refer to the Global Optimisation Toolbox documentation (MathWorks, 2025a).

The final welding process parameters were selected from the Pareto front by adapting the distance criterion to our conditions. This is a popular method for calibrating classification models and enables the selection of the ROC curve threshold point (Awtoniuk et al., 2022; Perkins & Schisterman, 2006). The criterion was applied in two variants: without normalisation (5) and with normalisation (6). The smallest value of the distance criterion (d) indicated the target parameters of the welding process. Furthermore, the parameters indicated by the criterion, both with and without normalisation, were verified.

$$d = [y_{MI} - \min(y_I)]^2 + [y_{MF} - \max(y_F)]^2 \tag{5}$$

$$d = \left[\frac{y_{MI} - \min(y_I)}{\max(y_I) - \min(y_I)}\right]^2 + \left[\frac{y_{MF} - \min(y_F)}{\max(y_F) - \min(y_F)} - 1\right]^2 \tag{6}$$

Where: y_{MI} – the vector of model M_I output values, y_I – the vector of measured welding current values, y_{MF} – the vector of model M_F output values, y_F – the vector of measured maximum force values.

3. RESULTS

Modifying welding parameters can affect the microstructure and properties of joints. Therefore, prior to strength testing (pull-off testing), the samples were characterised using visual inspection, metallography and hardness testing.

3.1. Microstructural characterisation and hardness measurements of welded joints

Heat-affected zone analysis was performed on 30 specimens, and the results for one sample are shown in Figures 9 and 10. As can be seen in Figure 9, the macrostructure cross-sections clearly show a noticeable difference in the size of the heat-affected zone (HAZ) for samples produced under different welding parameters. The difference in HAZ size was calculated using CAD software. The sample in Figure 9a was produced using a long welding time (600 ms) and low power (11.5 kW), while the sample in Figure 9b was produced using high power (19.5 kW) and a very short welding time (60 ms). Consequently, the sample shown in Figure 9b had a HAZ that was 2.5 times smaller than that shown in Figure 9a. Similar results were observed in the macrostructural analysis of samples produced using different welding technologies. According to the literature (Eshraghi et al., 2014), increasing the welding current or time can lead to a larger HAZ in steel joints.

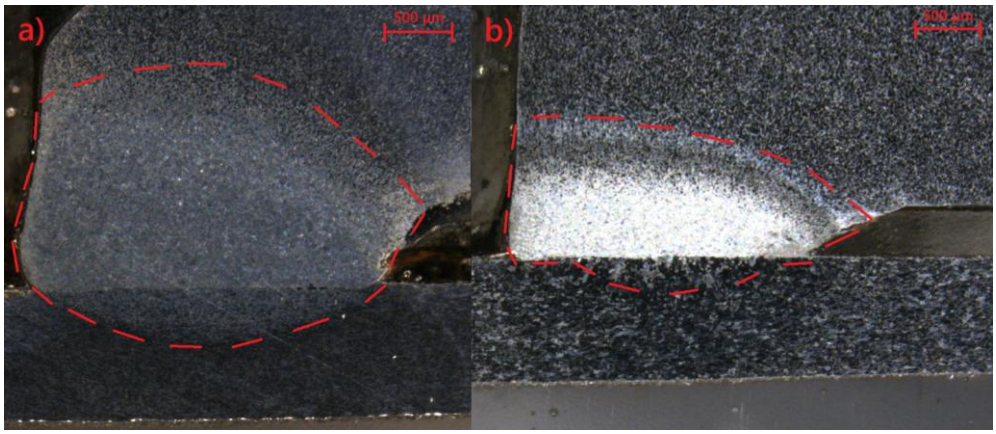

Fig. 8. Macroscopic comparison of the joint cross-sections of the hazard-affected zones and weld nuggets: (a) Sample No. 17; and (b) sample no. 49, which were welded using different parameters (see text for details)

The microstructure of the welded joint was analysed to determine any structural changes to the weld nugget. Figure 10 illustrates the areas that were examined, including the nut, the heat-affected zone, the weld nugget and the sheet metal. The ferritic-pearlitic structure of the nugget is clearly visible (Fig. 10). Figure 11a is a typical structure for low-carbon sub-eutectoid steel, with the ferrite phase dominating. Figures 11b and 11c visualise the pearlite grains with the characteristic lamellar morphology of ferrite and cementite in a ferritic matrix. During projection welding, the material undergoes rapid heating and cooling, with the thermal action primarily affecting the area of the nut projection (Mikno, 2018; Wang & Zhang, 2017). These factors significantly influence the macro- and microstructure observed in the weld cross-section. Figure 12 shows the transition zone between the nut and the weld.

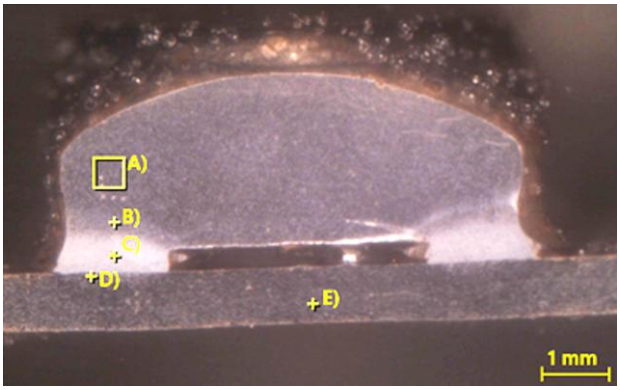

Fig. 9. The macrostructure of the nut-sheet weld joint, with the areas marked for microstructure analysis, is shown in the figs. 11–14: A – nut; B – HAZ (nut-weld area); C – weld; D – HAZ (weld-sheet metal area); E – sheet metal, polished and etched using Nital

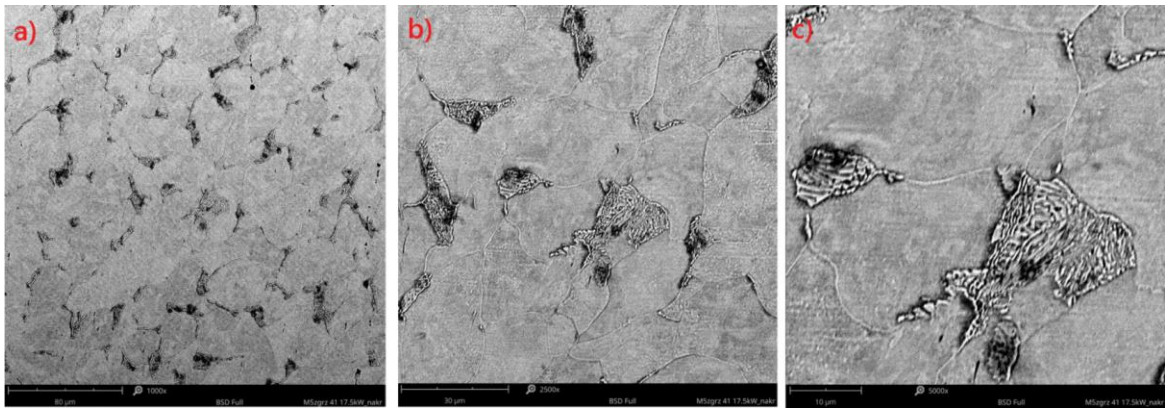

Fig. 10. The microstructure of a nut (area A in Fig. 10): (a) 1000x; (b) 2500x; (c) 5000x, SEM

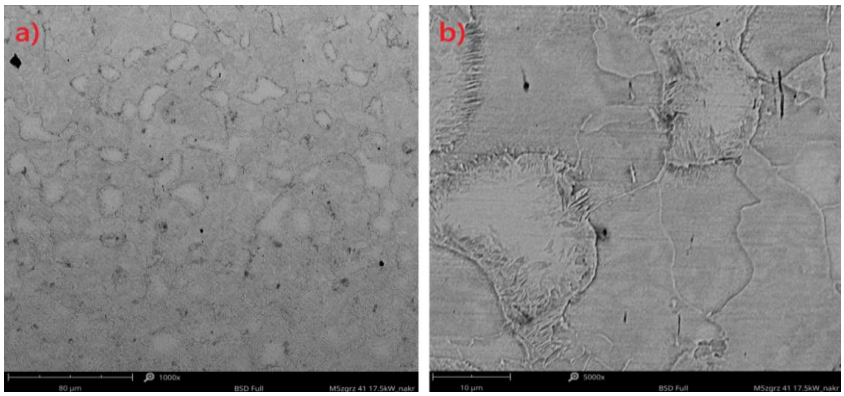

Fig. 11. The microstructure of the heat-affected zone between the nut and weld (area B in fig. 10): (a) 1000x; (b) 5000x, SEM

Figure 12 shows visible ferrite grains and areas of ferrite supersaturated with carbon (corresponding to former pearlite grains that transformed into austenite during welding). This is the area of the weld where the steel cooled relatively quickly and presumably did not reach the Ms temperature (martensite start temperature). As the cooling process took place below A_{r3}, the martensitic transformation could not occur throughout the entire volume of the structure, thus only bainitic transformation occurred. It is believed that acicular bainitic structures form at the grain boundaries in carbon-saturated ferrite areas (created from former pearlite areas during heating and supersaturated by carbon during cooling). Therefore, in the weld (Fig. 13), martensite formed, and the proportion of bainite decreased. The cooling rate during welding was sufficient to mitigate both carbon diffusion and bainite transformation. Conversely, in areas of the heat-affected zone distant from the weld nugget in steel (Fig. 12), the temperature A_{r3} was not reached.

Inside the weld nugget (Fig. 13), a martensitic structure forms, characterised by martensite needles at 60°. This occurs because the weld nugget cools at a rate greater than the critical rate. This blocks the diffusional transformation of austenite into more ordered equilibrium structures, such as pearlite or ferrite. The weld nugget shown in Figures 13b and 13c is characterised by a martensitic-ferritic microstructure (with martensite in the majority). It can be assumed that the weld underwent a partial hardening process in the $A_3 - A_1$ and temperature range, resulting in a martensitic-ferritic structure. A higher martensite-to-ferrite ratio hardens the steel (Khorasani et al., 2023). Based on observations of the steel microstructure, a low carbon content was found. As is well known, the lower the carbon content in steel, the greater the undercooling necessary to obtain a martensitic structure. Similar behaviour to that reported for area B in Figure 12 was observed in area D in Figure 10, which is enlarged in Figure 14.

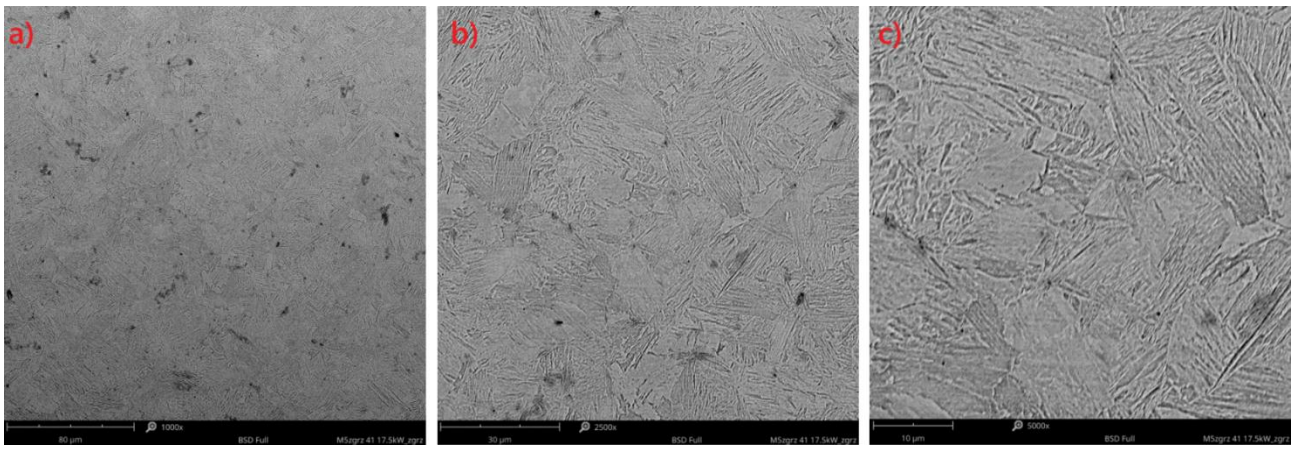

Fig. 12. Weld nugget microstructure (area C in fig. 10): (a) 1000x; (b) 2500x; (c) 5000x, SEM

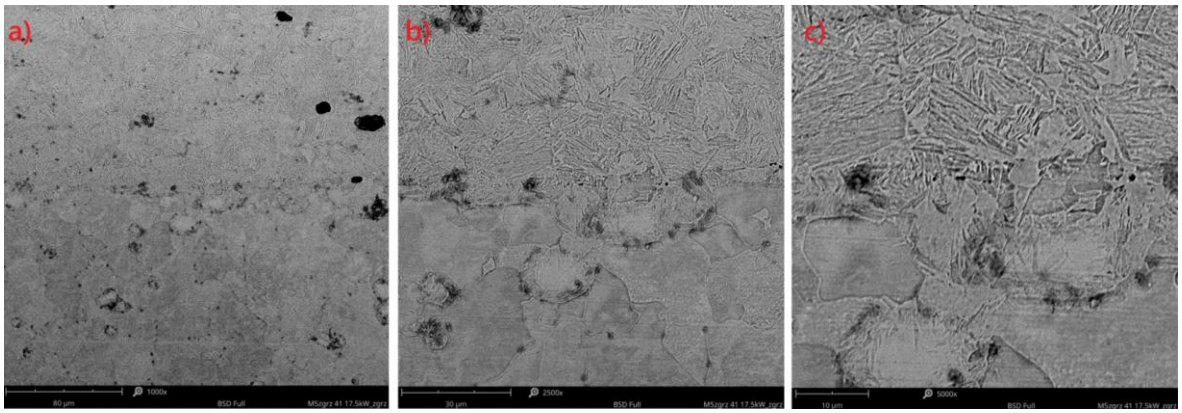

Fig. 13. The microstructure of the transition zone between the weld nugget and sheet metal (area D in fig. 10): (a) 1000x; (b) 2500x; (c) 5000x, SEM

Figure 14 clearly shows the connection between the nut and the sheet. The weld is formed primarily in the projections of the nut. The significant difference in structure and hardness (Tab. 1) may indicate a difference in chemical composition between the nut and the steel sheet. For example, the S235JR sheet has a significantly lower carbon content (nominally 0.17% C) than the nut (more than 0.17% C). At the interface between the nut and the metal sheet, a martensitic-ferritic structure forms on the sheet metal side. The thermal cycle of welding causes the weld to form in the area of the projections. This area undergoes the most significant microstructural changes due to temperature fluctuations in a relatively small volume of the projection, relating to the melting and solidification of the weld nugget metal. The sheet metal to which the nut is attached melts to a much lesser extent than the nut's projections.

The microstructure of the sheet metal visible in Figure 14 is characterised by a ferritic structure with fine pearlite grains, which is typical of mild steel (Zając et al., 2022). The S235JR mild steel sheet structure contains less pearlite than the nut, indicating a lower carbon content. Therefore, the hardness of the sheet metal ranges from 112 to 127 HV0.3 (Tab. 1), which is lower than the hardness of the nut, which is reported to range from 179 to 215 HV0.3. This is consistent with the observation that steels with a higher carbon content are harder (Szala et al., 2023). Microstructural analyses confirm that the hardness of the obtained weld nugget oscillates within the range of 300–400 HV0.3 (Tab. 1), which is characteristic of low-carbon martensite hardness and consistent with the hardness reported for low-carbon martensitic ferritic steel (Tóth, 2021; Zamani et al., 2022). Hardness analysis of both nuts (M4 and M5), as presented in Table 1, shows that it is impossible to determine whether welding time or welding power has a greater influence on joint hardness.

Tab. 1. Exemplary welding parameters and Vickers hardness measured in the specific joint areas: sheet metal, nut and weld nugget of joints made with M5 and M4 nuts

Welding parameters for nut M5								
Sample no. 6			Sample no. 36			Sample no. 41		
Power, P [kW]	Time, t [s]		Power, P [kW]	Time, t [s]		Power, P [kW]	Time, t [s]	
10	0.1		15	0.06		16,25	0.06	
Localisation of Vickers hardness measurement, HV0.3								
Sheet	Nut	Weld	Sheet	Nut	Weld	Sheet	Nut	Weld
122±12	198±5	408±21	111±23	215±8	303±72	112±6	204±6	388±37
Welding parameters for nut M4								
Sample no. 5			Sample no. 30			Sample no. 9		
Power, P [kW]	Time, t [s]		Power, P [kW]	Time, t [s]		Power, P [kW]	Time, t [s]	
16.25	0.1		25	0.02		17.5	0.06	
Localisation of Vickers hardness measurement, HV0.3								
Sheet	Nut	Weld	Sheet	Nut	Weld	Sheet	Nut	Weld
127±15	179±3	340±13	119±7	191±8	349±9	120±4	211±9	316±11

3.2. Weld strength testing results

The graphs shown in Figure 15 were prepared based on the results of the strength tests. All tests were performed according to the procedure presented in Figure 4. Figure 15a shows the relationship between maximum force and welding power. This figure demonstrates an upward trend, with the highest single value recorded at 70% of the welder's maximum power. A similar pattern is observed between force and welding current, as illustrated in Figure 15b. This similarity is because the applied power primarily influenced the welding current during the trial. Figure 15b also suggests that welding currents above 10 kA may negatively affect joint quality. However, this is of limited practical importance as nuts begin to deform at such current levels and cannot be used for further testing.

Figure 15c shows the relationship between maximum force and welding time. It can be seen that shorter welding times tend to produce better results in strength tests (higher force values). The number of samples tested at longer welding times is significantly lower than at shorter times. This is because it is difficult to achieve a satisfactory joint between the nut and the sheet without severely deforming the nut.

As current flows for longer, the nut's thread absorbs more heat and deforms substantially, making it difficult to obtain repeatable results at longer welding times. Finally, Figure 15d shows the maximum force in relation to the electrode pressure.

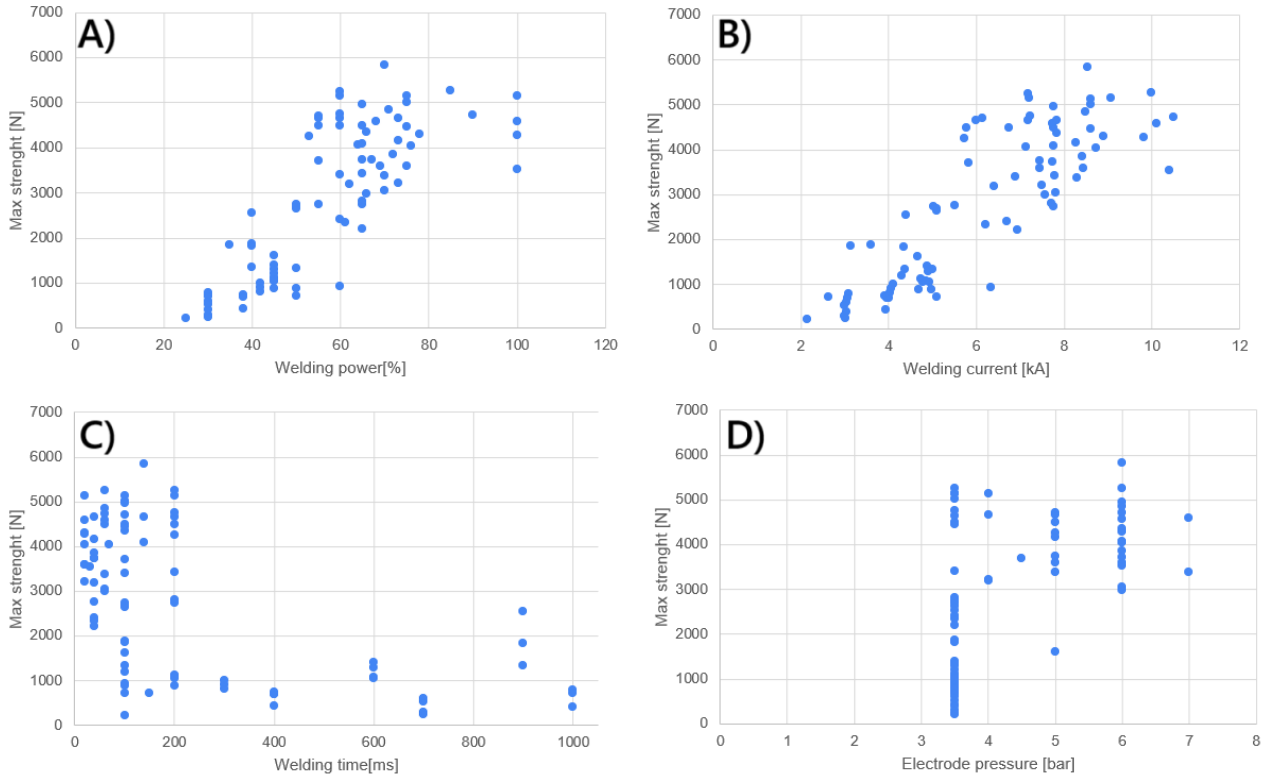

Fig. 14. Relationships between model input and output variables:
(a) welding power on the maximum nut pull-off strength; (b) welding current on the maximum nut pull-off strength;
(c) welding time on the maximum nut pull-off strength; (d) electrode pressure on the maximum nut pull-off strength

3.3. Model development and process optimisation

Table 2 shows the results of hyperparameter optimisation for the M_F and M_I models during the learning process. Table 3 contains an evaluation of the performance of optimised model structures using the MAE indicator. See the Statistics and Machine Learning Toolbox documentation (Mathworks, 2025b) for a detailed description of hyperparameters.

Tab. 2. Hyperparameter optimisation results of the models

Hyperparameter name	Search Range	Optimised values	
		M_F	M_I
number of learners	10-500	94	202
learning rate	0.001-1	0.28752	0.2255
minimum leaf size	1-33	9	1
maximum number of splits	1-66	66	3
number of predictors to sample	1-4	2	4

Tab. 3. Model performance metrics

Model	MAE	
	Learning dataset	Testing dataset
M_F	332.6 N	484.1 N
M_I	0.023 kA	0.174 kA

Figure 16 shows the Pareto front, which represents a set of optimal solutions. Using the distance criteria (5 and 6), two cases were selected for experimental verification for each of the M4 and M5 nuts. Table 4 shows the optimised technological process parameters.

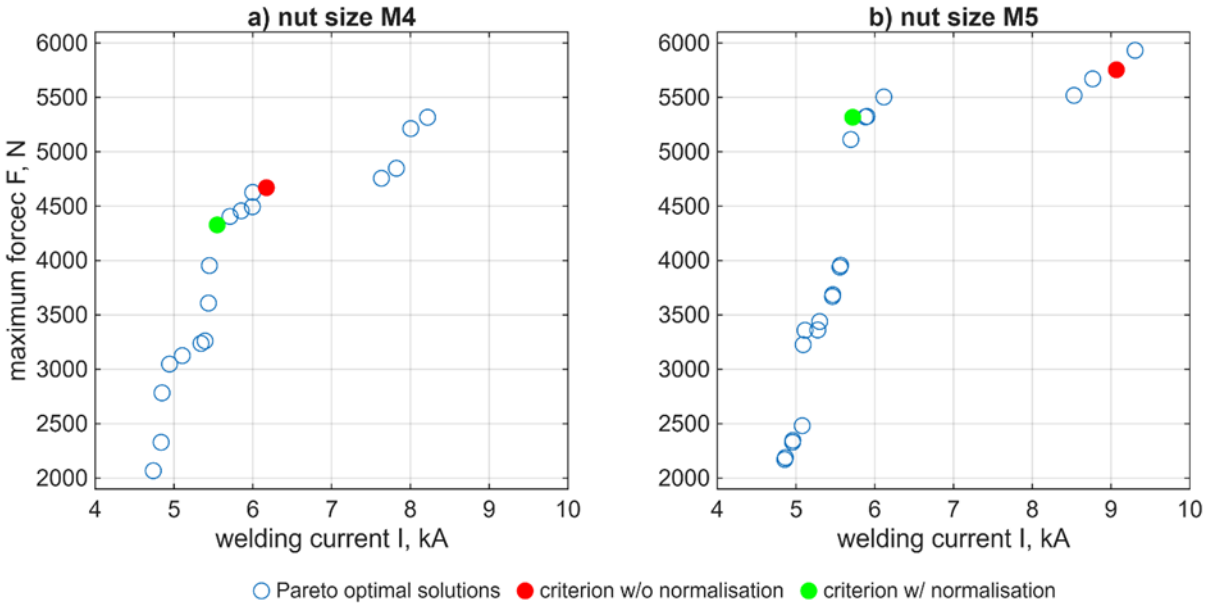

Fig. 15. The Pareto front in the objective plane in case of nut size: (a) M4; (b) M5

Tab. 4. Optimised projection resistance welding technological parameters

Nut size	Technological parameters		
	Electrode pressure *p* [bar]	Welding power *P* [kW]	Welding time *t* [ms]
M4*	5.8	12.875	120
M4**	4.4	13.125	60
M5*	6.4	18.750	240
M5**	4.4	12.875	180

* denotes parameters obtained using the distance criterion without normalisation
** denotes parameters obtained using the distance criterion with normalisation

3.4. Empirical verification of optimised technological parameters

Based on the results of the model, samples were produced using the parameters suggested by the algorithm. To verify the accuracy of the algorithm, a strength test was conducted on these samples using the same

procedure as for the samples in the training dataset. This process was repeated three times for each set of parameters. The results are presented in Table 5.

Tab. 5. Exemplary results of empirical verification of optimised welding parameters

Nut size	Maximum force *F* [N]		Welding current *I* [kA]		Weld crack
	y_F	y_{MF}	y_I	y_{MI}	
M4*	4306	4670	5.28	6.2	0
	3791		5.47		0
	3518		5.35		0
M4**	3483	4327	5.36	5.5	0
	3145		5.5		0
	2880		5.37		1
M5*	-	5754	8.9	9.1	-
	-		8.94		-
	-		8.96		-
M5**	3696	5318	5.33	5.7	1
	3688		5.11		1
	4047		5.2		0

* denotes parameters obtained using the distance criterion without normalisation
** denotes parameters obtained using the distance criterion with normalisation

Based on experimental verification, it is impossible to determine unequivocally whether selecting the optimal solution from the Pareto front with or without normalisation is better. For the M4 nut, however, a more accurate prediction of the welding current was obtained using the normalised criterion. In one iteration, the model accurately predicted the value of the output signal. The average relative error across three iterations was approximately 1.7%. By contrast, a more accurate result was obtained for the variant without normalisation in the maximum force prediction. The minimum relative error was 8.5%, and the average error across three iterations was 21.5%.

A more accurate prediction of the M5 nut's welding current was obtained without normalisation. The relative errors were consistent across all iterations, averaging at 1.9%. However, we could only assess the maximum force prediction for the variant with normalisation. In three repetitions, the mean relative error was 39.8%. The strength test could not be performed on the M5 sample set (without normalisation) as all the samples were deformed, making the test impossible to conduct. As the algorithm did not account for deformation, it selected a longer welding time. This parameter significantly impacts the shape retention of the nut during the process and must therefore be appropriately limited during sample production.

The maximum force prediction was associated with larger error values. This was due to greater scatter in the data across the three repetitions. The weld crack column in Table 5 indicates samples in which the weld nugget fractured. These samples exhibited a substantial reduction in joint strength, resulting in a greater disparity between the predicted and actual force values.

A similar methodology is presented in Johnson et al. (2023). The authors report an average relative error of 2.71% for the tensile shear strength and peel strength model outputs from the experimental verification stage. However, the process settings were drawn from the entire set to form the Pareto front. Our methodology proposes a measurable criterion for selecting the optimal solution. The quality of the prediction can be improved, however, by incorporating qualitative sample classification information into the model structure. The current model, shown in Figure 8, has two prediction modules. In future studies, it would be worthwhile considering adding a third module: a classification module. Incorporating additional qualitative information about the sample into the objective function (Eqn. 9) would enable the optimisation algorithm to work more effectively.

4. CONCLUSIONS

The study employed computer modelling to determine the optimal process parameters for resistance projection welding, advancing the optimisation of these parameters using the original procedure. This detailed modelling process helped minimise energy consumption (welding current) while maximising joint strength

(pull-off test results), the primary aim of the work. The set of optimised welding parameters identified by AI was verified through experimental final strength testing, including sample welding and strength testing. The findings of the present study led to the following conclusions:

- A model with input signals of nut size, electrode pressure, welding power, and welding time is sufficient for predicting welding current values. However, to improve the accuracy of maximum force prediction, the model should be expanded with additional input signals, such as the indentation of the welding electrode into the material.
- The proposed distance criterion is a valuable tool for selecting the optimal welding process parameters from a set of Pareto-optimal solutions.
- The model should include a qualitative assessment of the completed sample to avoid finding unfeasible solutions, such as nut damage.
- Based on the distance criterion, we determined the optimal welding process parameters for the M4 nut as electrode pressure of 4.4 bar; welding power of 13.125 kW; and welding time of 60 ms. The sample obtained with these parameters exhibited the following properties: maximum force of 3169±247 N and welding current of 5.41±0.064 kA.
- Based on the distance criterion, we determined the optimal M5 nut welding parameters as follows: electrode pressure of 4.4 bar; welding power of 12.875 kW; and welding time of 180 ms. The sample obtained with these parameters exhibited the following properties: a maximum force of 3594 ± 138 N and a welding current of 5.19 ± 0.1 kA.

Overall, superior welding joints were achieved with short welding times and high power – commonly known as hard-welding parameters. Nuts welded under these conditions did not deform, and the welding joints easily withstood forces applied in pull-off testing that exceeded the nominal yield strength of the sheet metal (S235JR). Furthermore, joints produced with short welding times demonstrated limited heat-affected zones and lower hardness values (e.g., a sample welded for a long time had a hardness of 408 HV0.3, whereas a sample welded for a shorter time had a hardness of 314 HV0.3). The increase in hardness of the weld compared to the base material was due to the transformation of the ferritic-pearlitic microstructure into a martensitic-ferritic structure within the weld nugget.

Conflicts of interest

The authors declare no relevant conflicts of interest pertaining to the content of this work.

REFERENCES

Antosz, K., Kulisz, M., & Husar, J. (2024). Evaluation and comparison of selected machine learning methods for improving maintenance processes. *IFAC-PapersOnLine*, *58*(8), 85–90. https://doi.org/10.1016/j.ifacol.2024.08.055

Awtoniuk, M., Majerek, D., Myziak, A., & Gajda, C. (2022). Industrial application of deep neural network for aluminum casting defect detection in case of unbalanced dataset. *Advances in Science and Technology. Research Journal*, *16*(5), 120–128. https://doi.org/10.12913/22998624/154963

Breiman, L. (2001). Random forests. *Machine Learning*, *45*(1), 5–32. https://doi.org/10.1023/A:1010933404324

Chuenmee, N., Phothi, N., Chamniprasart, K., Khaengkarn, S., & Srisertpol, J. (2025). Machine learning for predicting resistance spot weld quality in automotive manufacturing. *Results in Engineering*, *25*, 103570. https://doi.org/10.1016/j.rineng.2024.103570

Drégelyi-Kiss, Á. (2023). On the optimisation of the resistance projection welding process. *Material and Mechanical Engineering Technology*, *3,* 3–10. https://doi.org/10.52209/2706-977X_2023_3_3

Dziurka, R., Stanisz, D., Parzych, S., Zbyrad-Kołodziej, W., & Bochenek, M. (2025). Assessing electrode wear: The role of spot weld count in material degradation. *Advances in Science and Technology. Research Journal*, *19*(9), 369–384. https://doi.org/10.12913/22998624/207858

Eshraghi, M., Tschopp, M. A., Asle Zaeem, M., & Felicelli, S. D. (2014). Effect of resistance spot welding parameters on weld pool properties in a DP600 dual-phase steel: A parametric study using thermomechanically-coupled finite element analysis. *Materials & Design (1980-2015)*, *56*, 387–397. https://doi.org/10.1016/j.matdes.2013.11.026

Han, G., Ha, S., Marimuthu, K. P., Murugan, S. P., Park, Y., & Lee, H. (2021). Shape optimisation of square weld nut in projection welding. *The International Journal of Advanced Manufacturing Technology*, *113*(7–8), 1915–1928. https://doi.org/10.1007/s00170-021-06771-7

Hastie, T. J., Tibshirani, R., & Friedman, J. H. (2009). *The elements of statistical learning: Data mining, inference, and prediction* (2nd ed). Springer.

Hu, J., Bi, J., Liu, H., Li, Y., Ao, S., & Luo, Z. (2022). Prediction of resistance spot welding quality based on BPNN optimised by improved sparrow search algorithm. *Materials*, *15*(20), 7323. https://doi.org/10.3390/ma15207323

Johnson, N. N., Madhavadas, V., Asati, B., Giri, A., Hanumant, S. A., Shajan, N., & Arora, K. S. (2023). Multi-objective optimisation of resistance spot welding parameters of BH340 steel using kriging and NSGA-III. *Transactions of the Indian Institute of Metals*, *76*(11), 3007–3020. https://doi.org/10.1007/s12666-023-03051-8

Khorasani, F., Jamaati, R., & Aval, H. J. (2023). A low-cost strategy to improve strength-ductility-toughness balance in a low-carbon steel. *Ironmaking & Steelmaking*, *50*(9), 1340–1351. https://doi.org/10.1080/03019233.2023.2208988

Kik, T., Górka, J., Kotarska, A., & Poloczek, T. (2020). Numerical verification of tests on the influence of the imposed thermal cycles on the structure and properties of the S700MC heat-affected zone. *Metals*, *10*(7), Article 7. https://doi.org/10.3390/met10070974

Koal, J., Baumgarten, M., Nikolov, C., Ramakrishnan, S., Mathiszik, C., & Schmale, H. C. (2025). Acoustic process monitoring during projection welding using airborne sound analysis and machine learning. *Welding in the World*, *69*, 459–470. https://doi.org/10.1007/s40194-024-01876-5

Korzeniowski, M., Małachowska, A., Biały, M., Kanczewska, M., Tkaczyk, M., & Grajczyk, K. (2023). Experimental investigation on an algorithm for testing the quality of powder distribution during 3D printing process. *Advances in Science and Technology. Research Journal*, *17*(5), 289–301. https://doi.org/10.12913/22998624/171809

Kubit, A., Macek, W., Zielecki, W., Szawara, P., & Kłonica, M. (2023). Fracture surface topography parameters for S235JR steel adhesive joints after fatigue shear testing. *Advances in Science and Technology. Research Journal*, *17*(5), 130–139. https://doi.org/10.12913/22998624/171490

Larsson, J. (2008). Projection welding for nut and bolt attachment. The Fabricator. https://www.thefabricator.com/thefabricator/article/shopmanagement/projection-welding-for-nut-and-bolt-attachment

Łatka, L., Pawłowski, L., Winnicki, M., Sokołowski, P., Małachowska, A., & Kozerski, S. (2020). Review of functionally graded thermal sprayed coatings. *Applied Sciences*, *10*(15). https://doi.org/10.3390/app10155153

Masoudi Nejad, R., Sina, N., Ma, W., Song, W., Zhu, S. P., Branco, R., Macek, W., & Gholami, A. (2024). Artificial neural network-based fatigue life assessment of riveted joints in AA2024 aluminium alloy plates and optimisation of riveted joints parameters. *International Journal of Fatigue*, *178*, 107997. https://doi.org/10.1016/j.ijfatigue.2023.107997

Mathworks. (2025a). *Global Optimisation Toolbox User's Guide*.

Mathworks. (2025b). *Statistics and Machine Learning Toolbox User's Guide*.

Mikno, Z. (2018). Projection welding of nuts involving the use of electromechanical and pneumatic electrode force. *The International Journal of Advanced Manufacturing Technology*, *99*(5–8), 1405–1425. https://doi.org/10.1007/s00170-018-2525-5

Mikno, Z., Kowieski, S., & Pilarczyk, A. (2019). Projection welding of nuts with full projections with use of electromechanical operating force system. *Biuletyn Instytutu Spawalnictwa w Gliwicach*, *63*(2), 7–16. https://doi.org/10.17729/ebis.2019.2/1

Nielsen, C. V., Zhang, W., Martins, P. A. F., & Bay, N. (2014). Numerical and experimental analysis of resistance projection welding of square nuts to sheets. *Procedia Engineering*, *81*, 2141–2146. https://doi.org/10.1016/j.proeng.2014.10.299

Perkins, N. J., & Schisterman, E. F. (2006). The inconsistency of "optimal" cutpoints obtained using two criteria based on the receiver operating characteristic curve. *American Journal of Epidemiology*, *163*(7), 670–675. https://doi.org/10.1093/aje/kwj063

Russell, M., Kershaw, J., Xia, Y., Lv, T., Li, Y., Ghassemi-Armaki, H., Carlson, B. E., & Wang, P. (2024). Comparison and explanation of data-driven modelling for weld quality prediction in resistance spot welding. *Journal of Intelligent Manufacturing*, *35*(3), 1305–1319. https://doi.org/10.1007/s10845-023-02108-1

Sawa, M., Szala, M., & Henzler, W. (2021). Innovative device for tensile strength testing of welded joints: 3d modelling, FEM simulation and experimental validation of test rig – a case study. *Applied Computer Science*, *17*(3), 92–105. https://doi.org/10.23743/acs-2021-24

Singh, J., Vasudev, H., Szala, M., & Gill, H. S. (2024). Neural computing for erosion assessment in Al-20TiO2 HVOF thermal spray coating. *International Journal on Interactive Design and Manufacturing (IJIDeM)*, *18*(4), 2321–2332. https://doi.org/10.1007/s12008-023-01372-y

Stavropoulos, P., & Sabatakakis, K. (2024). Quality assurance in resistance spot welding: state of practice, state of the art, and prospects. *Metals*, *14*(2). https://doi.org/10.3390/met14020185

Szala, M., & Łukasik, D. (2018). Pitting corrosion of the resistance welding joints of stainless-steel ventilation grille operated in swimming pool environment. *International Journal of Corrosion*, *2018*(1). https://doi.org/10.1155/2018/9408670

Szala, M., Łatka, L., Awtoniuk, M., Winnicki, M., & Michalak, M. (2020). Neural modelling of APS thermal spray process parameters for optimising the hardness, porosity and cavitation erosion resistance of Al2O3-13 wt% TiO2 coatings. *Processes*, *8*(12), 1544. https://doi.org/10.3390/pr8121544

Szala, M., Szafran, M., Matijošius, J., & Drozd, K. (2023). Abrasive wear mechanisms of S235, S355, C45, AISI 304, and Hardox 500 steels tested using garnet, corundum and carborundum abrasives. *Advances in Science and Technology. Research Journal*, *17*(2), 147–160. https://doi.org/10.12913/22998624/161277

Tóth, L. (2021). The possibilities of the retained austenite reduction on tool steels. *Crystal Engineering*, *6*(2), 99–105. https://doi.org/10.36868/ejmse.2021.06.02.099

Wang, X., & Zhang, Y. (2017). Effects of welding procedures on resistance projection welding of nuts to sheets. *ISIJ International*, *57*(12), 2194–2200. https://doi.org/10.2355/isijinternational.ISIJINT-2017-219

Winiczenko, R., Salat, R., & Awtoniuk, M. (2013). Estimation of tensile strength of ductile iron friction welded joints using hybrid intelligent methods. *Transactions of Nonferrous Metals Society of China*, *23*(2), 385–391. https://doi.org/10.1016/S1003-6326(13)62474-7

Zając, K., Płatek, K., Wachel, P., & Łatka, L. (2022). Fractal dimension as robust estimate of low carbon steels hardness. *Advances in Science and Technology. Research Journal*, *16*(5), 335–344. https://doi.org/10.12913/22998624/155799

Zamani, M., Ghasemi, H. M., & Mirzadeh, H. (2022). Effect of variation of martensite with a constant carbon content on mechanical behavior and sliding wear of dual phase steels. *Tribology Letters*, *70*(73). https://doi.org/10.1007/s11249-022-01616-0